Indian Journal of Geo Marine Sciences
Vol. 51 (04), April 2022, pp. 310-321

Evaluation and performance of satellite-derived bathymetry algorithms in turbid coastal water: a case study of Vengurla rocks

M Ashphaq*[,a], P K Srivastava[b] & D Mitra[c]

[a]National Hydrographic Office, Dehradun – 248 001, India

[b]University of Petroleum & Energy Studies (UPES), Dehradun – 248 007, India

[c]Indian Institute of Remote Sensing, Dehradun – 248 001, India

*[Email: ashphaq.md824@nic.in]

Received 06 October 2021; revised 23 April 2022

The coastal region bathymetry is increasingly becoming necessary for emerging needs of navigation and development along coasts. Satellite-Derived Bathymetry (SDB) has been examined as a viable alternative for hydrographic surveys for the past few decades to reduce the data acquisition efforts in coastal regions and augmentation of periodic updating of Electronic Navigational Charts (ENCs). The previous studies have applied SDB algorithms in less complex waters due to the limitations of SDB algorithms in turbid and varying shallow waters. This paper analyses three different medium-resolution satellite imagery data to derive bathymetry in a navigably very complex and highly turbid region, Vengurla rocks, situated on the west coast of India. The objective of the study was to evaluate the best suitable technique for SDB in turbid water. The bathymetry product images have been derived using the two most commonly utilized log ratio, and linear ratio transformation; three semi-automated methods, Principal Component Analysis (PCA), Independent Component Analysis (ICA), and ratio transform; and Machine Learning (ML) regression algorithms. Among the applied transform and algorithms, the ML algorithm using 561 nm band data performed the best, resulting in R^2 of 0.77, RMSE of 3.4 m, and MAE of 2.8 m. This work established that open source images of sensor OLI/Landsat-8 satellite provide the best results of SDB estimation in complex turbid water by applying ML algorithms. However, extreme turbid and complex regions resulted in more erroneous SDB estimation specifying the need for refining algorithms using bio-optical parameters.

[**Keywords**: Bathymetry, Coastal region, Depth estimation, Machine learning, Satellite-derived bathymetry]

Introduction

The importance of bathymetric studies is manifested in its vast application areas, including marine navigation, near-shore constructions, harbours, submarine pipelines & cable laying, and so on. Traditionally, hydrographic surveying methods are used for bathymetric surveys carried by ship-based acoustic sounding. The traditional bathymetry procedures comprised depth measurements using sounding lead-line, pole log, and other such methods. The acoustic echo-sounding technology was the next step in the modernization of bathymetry techniques. The method used two different methodologies, Single Beam Echo Sounding (SBES) and Multi-Beam Echo Sounding (MBES), for depth and seabed topography determination. This development was further supplemented by evolving depth profilers, current profilers, oceanographic winches and other bio-optical sensors. Various contemporary approaches have recently been used to determine the ocean's bathymetry. This includes Light Detection and Ranging (LIDAR) operated from aerial platforms, ROVs (Remotely Operated Vehicles) & Autonomous Underwater Vehicles (AUVs) for effective determination of depth in coastal waters. Hydrographic surveying has a significant operating cost, which limits recurrent and frequent surveys in any region of interest. Furthermore, the scanning swath of echo sounders narrows in shallow water zones, reducing coverage. Because of the risk of losing men and materials, some remote and hazardous places, such as huge hidden reefs, streams, estuaries, tide bores, and surge zones, are very complicated to undertake hydrographic surveys. Remote and autonomous technologies like ROV & AUV are also costly for their high purchasing and maintenance costs.

This has led researchers, way back in the 1970s, to search for alternative methods to the bathymetric survey. SDB is one of the feasible alternatives that has been studied over the past five decades and successfully provides a major resolution to coastal regions characterized by rapid shoreline changes and

significant constraints areas where sparse or no data exists due to the complexity of surveying. The SDB technique was developed by Polcyn & Rollin[1] based on the theory of underwater reflectance using optical remote sensing data. Concurrently, the other group of researchers derived SDB using Satellite Altimetry data and Synthetic Aperture Radar (SAR) data. A log-linear empirical approach using single-band images for detecting SDB has been developed[2]. The research focused on removing all other reflected parameters that attenuate water bottom signals[3]. The chronological order of development of a few SDB algorithms commonly used is; Linear Band Model[3]; Flow Radiative Transfer Model[4]; the Depth of Penetration Zone (DOP) model[5]; and the mostly used Linear Ratio Model[6]. In the last decade, there was a surge in research on SDB and its applications[7]. The SDB provided alternately to bathymetry to evaluate coastal processes like erosion/ accretion, shoreline changes, underwater geomorphology, coastal wetlands, suspended sediment concentration, water quality, coastal habitats and other such activities. Also, Tsunami, like natural hazards, demands accurate bathymetry to model early warning detection[8]. Additionally, frequent knowledge of the rate of bathymetric changes for various reasons like construction of breakwater aids understanding of sediment pattern & rate of sediment transport[9] and marshy land detection[10]. Recent studies have used high-resolution satellite imagery data for depth retrieval using various ML, empirical and semi-analytical algorithms in turbid coastal water. Also, attempts have been made to explore potential areas of groundwater[11] and coastal marshland mapping[10] and land-use mapping using massive satellite data[12]. Recent advances in remote sensing in terms of higher resolution (spectral, spatial, radiometric & temporal), sensors evolving with several bands in the visible spectrum of Hyperspectral (HS) and MS (Multispectral) sensors, and numerous algorithms including artificial intelligence algorithms have improved the potential of SDB to be utilized as an alternative to bathymetric data.

This paper presents an analysis of open-source satellite images of Operational Land Imager (OLI) onboard Landsat-8 satellite, Multispectral Instrument (MSI) onboard Sentinel-2 (twin satellites A and B), and Advanced Spaceborne Thermal Emission and Reflection Radiometer (ASTER) onboard Terra satellite to derive bathymetry in navigably very complex and highly turbid water of Vengurla Rocks, situated at the west coast of India. The objective of the study was to evaluate the best suitable technique and satellite imagery for deriving SDB in the region. To fulfil the objective, a few commonly used SDB algorithms have been utilized for SDB derivation. The techniques employed include Multi-Linear Regression (MLR), Log Ratio Algorithm[6]; Log-Linear Model[13]; Semi-automated tools provided in Envi 5.3, Spectral Processing Exploitation and Analysis Software (SPEAR) relative bathymetry model, which includes PCA, ICA, and Log Ratio Algorithm. ML techniques, Linear Regression, have also been evaluated to derive SDB. In data analysis, bathymetry is regressed against the reflectance values in the selected few bands in the visible spectrum of ASTER/Terra, OLI/Landsat-8 and MSI/Sentinel-2 sensor images.

Material and Methods

Study area

This study area Vengurla (15°51’ N; 73°37’ E), is situated at the height of 1.2 m from the Mean Sea Level (MSL) in the Sindhudurg district of Maharashtra state of India. The coast of Vengurla consists of two headlands enclosing an embayed beach in between them. An alleviated sand dune runs parallel to the coast, beyond which casuarina plantation exists. Mangroves are located on both sides of the inlets of the Karli River. The nature of tides is largely semi-diurnal, with a tidal range of 1.3 m to 2.3 m. The Vengurla coast is harshly exposed to seasonal erosion due to the heavy waves during the monsoon[14]. Vengurla rocks is an archipelago consisting of 2 large hillocks or 18 big rocks and several small rocks. Vengurla rocks, located to the SW of Vengurla, is about 14 km long (West-North West) and 8.3 km wide, which is a habitat of several seabird species[15].

The presence of numerous visible and underwater rocks & obstructions has made this area unsafe for navigation. The nautical chart has demarcated the region as a foul area and unsafe for passage of vessels. However, the local fishermen community is well aware of navigational dangers and manoeuvres the boats clear of these underwater rocks. The area of Vengurla rocks has been selected to study its complexity to undertake a hydrographic survey, the presence of numerous underwater features to explore the highly turbid nature of water due to the outlet of Karli River carrying a discharge of sediments. All these challenges make this site ideal for assessing

SDB in the area. The Region of Interest (ROI) was cropped to fit the study area. The area included in the study is 208.46 sq. km covering a distance of around 12 km from the coast.

Data

Bathymetric data

From the surveying perspective, Vengurla rocks is a very complex and challenging area for carrying bathymetric surveys for the safety of surveying boats, instruments and hull-mounted sensors due to cliffy rocks and underwater dangers. The bathymetric survey in the area was carried out in February 2018 by single beam echo sounder Deso-30 using 210 kHz frequency. The Edgetech-4200-FSL Side-Scanner was used to identify shoals and obstructions for side-scanning in the underwater rock area. As per the survey order, the vertical accuracy achieved is 0.5 % of the total depth for the depth range of 0 to 32 m. The horizontal accuracy of 95 % confidence level, *i.e.*, 5 m + 5 % of water depth, is achieved using Differential Global Positioning System (DGPS). The bathymetric survey was having more than 26000 depth points, however, only 984 data representative samples were selected based on a 3 % margin of error and 95 % confidence interval. The train_test_split function was used in the scikit-learn library to create a randomized sample dataset. A total of 984 depth points were used for the study, out of which 50 % depth points were used for training, and 50 % depth points are used for testing the models. However, a final SDB evaluation was made for the entire bathymetric dataset.

Figure 1(a) below shows the sounding lanes in the survey area. The sounding lanes were carried perpendicular to the coast, and interlines were performed parallel to the beach. Figure 1(b) shows visible rocks in the area from the NIR band, and Figure 1(c) shows the Digital Terrain Model (DTM) depicting the several underwater rocks in the survey area.

Satellite data

The OLI/Landsat-8, MSI/Sentinel-2, and ASTER/Terra sensor satellite images are level 1 processed data, radiometrically calibrated, and orthorectified using Ground Control Points (GCP), and the Digital Elevation Model (DEM) has been downloaded using the USGS Earth Explorer tool. These three sensor image data are freely available and provide sufficient spatial resolution for SDB studies. OLI/Landsat sensor collects 30 m (15 m Pan) spatial resolution data and has 16 days revisit time having swaths of 185 km. The MSI/sentinel-2 sensor collects 10 m spatial resolution data with five days revisit time and 290 km swath. The ASTER/Terra has a 15 m spatial resolution with 16 days temporal resolution and 60 km swath width. The satellite data was downloaded for the close date of the bathymetric survey, except for ASTER/Terra (the best available image was in December 2016 for the site). Table 1 provides information on satellite data used in the study.

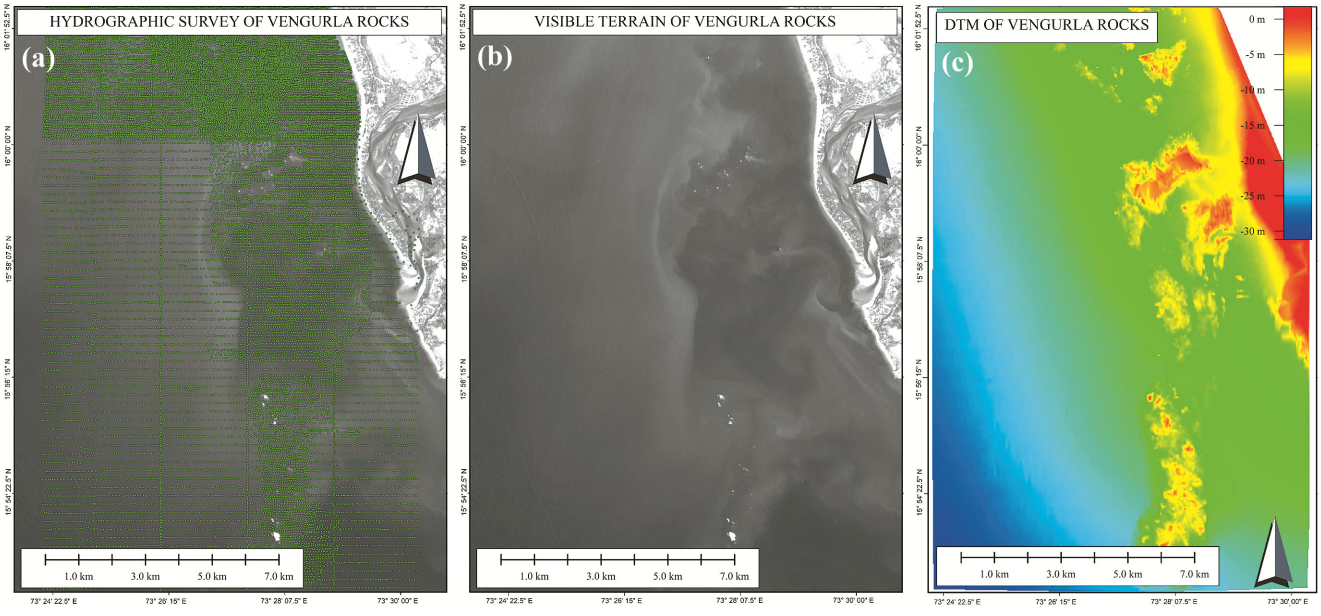

Fig. 1 — (a) Hydrographic survey, (b) Terrain in NIR band, and (c) DTM of Vengurla rocks

Table 1 — Details of satellite data bands used in the study

Band	Band name	Wavelength λ	Central λ	Bandwidth	Spatial resolution in m
OLI/LANDSAT-8		Image: LC08_L1TP_147049_20180227_20180308_01_T1 (12-Bits) Acquisition date of image used in the study: 27 Feb 2018			
2	Blue	450–515	482	60	30
3	Green	525–600	561	57	30
4	Red	630–680	654	37	30
5	NIR	845–885	864	28	30
MSI/ Sentinel-2		Image: S2A_MSIL1C_20180224T052811_N0206_R105_T43PCT (12-bits) Acquisition date of image used in the study: 24 Feb 2018			
2	Blue	448–546	490	65	10
3	Green	538–583	560	35	10
4	Red	646–684	665	30	10
8	NIR	763–908	842	115	10
ASTER/Terra		Image: AST_L1T_00312302016054611_20161231102100_17281 (8-Bits) Acquisition date of image used in the study: 31 Dec 2016			
1	Green	520-600	556	9	15
2	Red	630 – 690	661	6	15
3N	NIR	780-860	807	10	15

Principally, out of several spectral bands, most of the SDB studies have used blue and green bands for the SDB estimation[16]. This study aims to validate a few of the commonly used SDB algorithms in complex and turbid water of the Vengurla rocks. The objective is to achieve the goal where the optical satellite data image pixels may have corresponded to each depth point via suitable algorithms. The satellite images were selected based on coverage of the study site, cloud cover of less than 10 %, and the temporal proximity to the field survey. Also, images were filtered based on the effect of sun glint so that no correction is needed to enhance the image.

The OLI/Landsat-8 and MSI/Sentinel-2 sensor images are processed to 12-bits radiometric resolution providing enough variance in reflectance to estimate SDB. The radiometric resolution of ASTER/Terra imagery is 8 bits, providing significantly less variability in an image, especially in the area of the water region. The ASTER/Terra imagery does not have a blue band; hence the only available green and red bands have been analysed. The transect profile of the green band shows higher variability in reflectance than the red band; hence, only the green band of the ASTER sensor is used for applying the SDB algorithm.

Methodology

The methodology can be divided into broad stages; the first stage deals with downloading and pre-processing satellite imagery to remove the effect of the atmosphere by applying the Dark Object Subtraction (DOS) method and conversion from radiance to reflectance. Post image enhancement, a correlational analysis, has been carried out to select the most suitable band for SDB estimation. The second stage deals with applying different Transform and SDB algorithms, as shown in Figure 2.

The pre-processing of satellite imagery includes converting radiance measured at the sensor to the Top-of-Atmosphere (TOA) reflectance and then removing the atmospheric effect from TOA reflectance to get at the surface Bottom-of-Atmosphere (BOA) reflectance. Further, water column correction is applied to get underwater reflectance or sea-bottom reflectance in shallow water to derive SDB. Satellite sensors collect radiance information, which corresponds to the brightness in the direction of the sensor. The radiance information is used to calculate the reflectance (the ratio of reflected versus total emitted energy). The parameters used for calculation are provided in the metadata files are; at-satellite radiance, earth-Sun distance in astronomical units, mean solar exo-atmospheric irradiances, solar zenith angle and sun elevation degrees. The level-1 processed images are provided with 'scaled TOA reflectance', which can be converted to TOA reflectance. The effects of atmospheric gas particles and aerosol may be removed to calculate BOA reflectance, based on image-based techniques without any *in-situ* data. In the DOS method, it is assumed that the dark pixel in an image has no reflected light due to atmospheric scattering, as very few objects on the earth follow the principle of perfect blackbodies. Hence, atmospheric dispersion is removed by subtracting the dark pixels' value from each pixel in the band imagery. The TOA

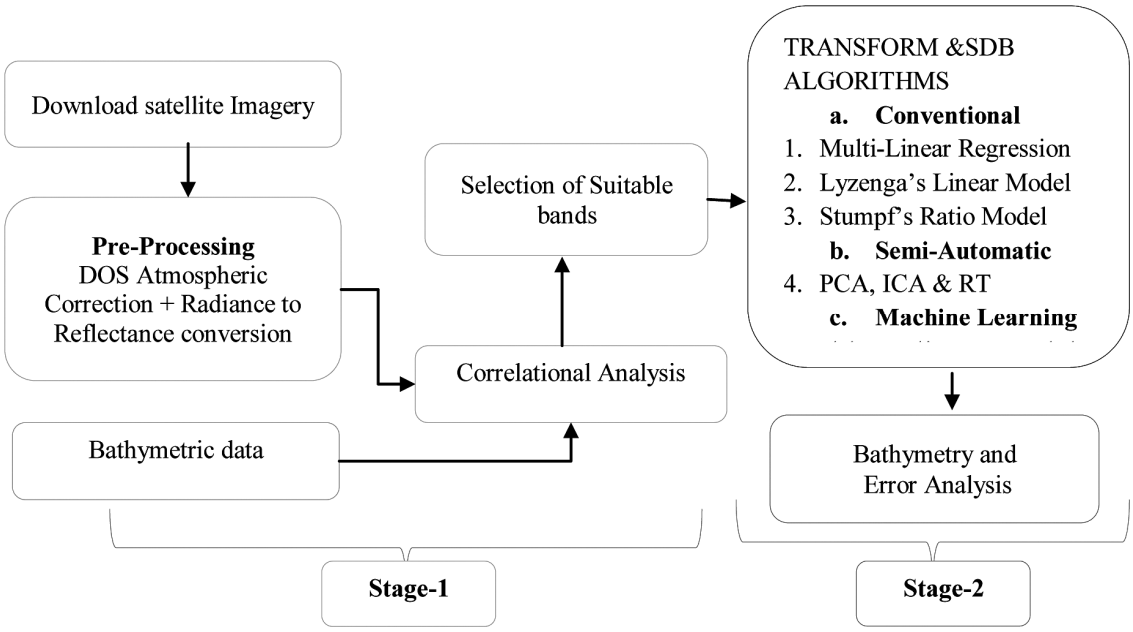

Fig. 2 — Flowchart of the methodology of the study

reflectance image is applied with DOS atmospheric corrections using the QGIS SCP plugin.

Radiometric calibration and atmospheric correction

The QGIS Semi-Automatic Classification Plugin (SCP) developed by Congedo[17] provides several automated solutions for downloading to processing satellite images. The QGIS SCP plugin has been used to carry out radiometric calibration of the satellite images. The SCP plugin reads the required parameter from the directory containing the data bands and metadata (.MTL) file. Simultaneously this tool performs DOS correction and saves the resultant product in the output directory. Thus, surface reflectance values were retrieved for further processing.

Correlational analysis

The correlation analysis between *in-situ* depth points and raw satellite images and pre-processed images were carried out for all three satellite images; however, only visual bands of ASTER sensor image were used for the analysis. The correlation analysis was intended to assess the best suitable bands for SDB estimation. The pixel values for corresponding depth points were extracted using European Space Agency's (ESA's) Sentinel Application Platform (SNAP) Desktop Application, and the correlation analysis was executed in MS Excel. The primary objective of the study was to assess the correlation of derived images with ground bathymetric data. The correlational analysis may reflect upon the best usable band data for further processing in such a complex site.

Transform and SDB algorithms

Log ratio transform

Log Ratio Transform technique was enhanced by Stumpf *et al.*[6], who suggested a Ratio of the attenuation of two bands (then using albedo) as different spectral bands attenuate at different rates. The algorithm derived is as given by Stumpf *et al.*[6]:

$$z = m_1 \frac{ln(nR_w(\lambda_j))}{\ln(nR_w(\lambda_i))} - m_0 \quad \text{... (1)}$$

Z - depth, n - constant to ensure the Ratio remains positive under all values, Rw is observed reflectance in a band, m_0 is the offset, and m_1 is a gain derived by regression.

This theory needs only *in-situ* calibration data, and results are independent of bottom type. However, the approach has been criticized for lack of physical foundation based on water optics and the selection of bands varies with site. Although the ratio of the blue and green band has been used for deriving coefficients. In this study, several ratio transforms have been compared using different Landsat band combinations.

Log-linear transform

The Radiative Transfer (RT) theory-based algorithms for water depth and bottom features extraction from single band exponential depth dependence was proposed using the *Log-Linear Transformation*[3,13]. This technique has an explanation for unpredictability in the bottom type by using multiple spectral bands. A variable, Xj, has been defined for each of the N bands[3]

$$z = h_0 - \sum_{J=1}^{N} h_j X_j \quad \ldots (2)$$

Where, $Xi = In(Li - Lsi)$; Lsi - deep-water radiance and Li- above-surface reflectance; h_j and h_0 was derived from regression of radiance and *in-situ* data. Deep-water reflectance was assumed to account for reflection from the sea surface, volume scattering in the water column and sun-glint effects, and atmospheric scattering.

PCA transform

The transform PCA is an orthogonal decomposition based on the covariance matrix of the Gaussian distribution of data. The PCA is used to reduce the dimensionality of data and transform an extensive data set into smaller variables representing information in a large dataset[18]. The set is of image bands such that the new bands (called components) are uncorrelated and ordered regarding the amount of variability they explain[19]. PCA adopts the first component from a study using all three bands (transformed) to correlate to water depth[19]. As the MS bands are highly correlated, the PC transformation is used to create uncorrelated component bands. PCA finds a new set of orthogonal axes which have the origin at the data mean and are rotated to maximize data variance. Thus, the resultant PC bands are uncorrelated and are also the linear combinations of the naive spectral bands. PC band contains the highest percentage of variance in data which decreases sequentially with each PC, such that the last PC shows very small variance mostly due to noise in the original data. The same number of output PC bands as input spectral bands can be calculated, however, only the first PC image has been used in the study as it was able to explain more than 90 % variance.

ICA transform

ICA is another well-known component mining technique that tries to identify independent sources underlying multispectral data. ICA uses higher-order statistics on the non-Gaussian assumption of the independent sources. The ICA provides the advantage of distinguishing features from the noisy bands (which are suppressed as the noise in PCA). The first IC image has been used in the study.

The Envi 5.3 Software has the tool SPEAR, which includes 'The Relative Water Depth tool' generating an image depicting relative water depth. This tool uses Blue, Green, Red and NIR bands to generate PCA transform, ICA transform, and Ratio algorithm products. These developed products were not calibrated to ground data, but only correlated to determine the best suitable product for further stages of study.

ML algorithm

SDB studies use ML initiated by Caballero *et al.*[20], using Artificial Neural Network (ANN) to derive SDB. Since then, different ML algorithms as per the context of the study have been implemented in SDB studies. In this study, Linear Regression techniques have been implemented using GUI-based Python IDE 'Jupytar Notebook' of Anaconda Navigator Distribution. The python libraries NumPy, Pandas, Geopandas, Scipy, sklearn (sklearn.linear_model, sklearn.neighbors) and Matplotlib, were used for data processing. The univariate regression equation is represented as

$$y = a + bx + \varepsilon \quad \ldots (3)$$

Where 'x' is the independent variable; 'y' is the dependant variable and 'ε' is a random error variable that affects y.

Error analysis

The accuracy of derived models was established by evaluating the SDB of derived images and regressing them against the validation data. The test dataset was used for validation and statistical parameters; the coefficient of determination R^2, the Root Mean Square Error (RMSE), and the Mean Absolute Error (MAE) were calculated for each method by the following procedure[7].

$$RMSE = \sum_{i=1}^{n} \sqrt{(x_i - y_i)^2 / n} \quad \ldots (4)$$

$$MAE = \frac{1}{n} \sum_{i=1}^{n} |x_0 - y_0| \quad \ldots (5)$$

Where, Xi is SDB derived from satellite imagery, and X_0 is the mean of SDB depths; Yi is *in-situ* validation depth, and y_0 is the mean of *in-situ* depth, n is total depth points

The quality of a regression model is measured using R^2 which allows the comparison of the

estimated model to a constant baseline (using data mean) and then determines how much better the estimated model is. R^2 will always have a value less than or equal to 1. The formula for R^2 is as follows[7]

$$R^2 = 1 - \frac{MSE(model)}{MSE(baseline)} \quad \ldots (6)$$

Results

Pre-processing

The open-source QGIS SCP was used for pre-processing of data. The correlation coefficients compared between the raw data and QGIS SCP processed data have shown only marginal enhancement. The correlation analysis has shown varying results for each band; however, no considerable improvement was seen in processed images compared to Level-1C processed images. The reason may be attributed to the accuracy of image pixel-based techniques which is usually lower than physical parameters-based corrections. Still, pixel-based techniques are valuable in the absence of atmospheric ground measurements. When the single image scene covers a vast area with a wide variation in ground characteristics or when the atmosphere is not uniform, the pixel-based techniques are less effective in removing the atmosphere effects.

The result of correlational analysis of *in-situ* depths to raw and QGIS SCP plugin processed images indicates that the green band is more highly correlated to depths than any other bands; hence only the green band is used in SDB estimation in Lyzenga's method and Machine Learning method. The blue band has the edge over the red band in all three-satellite data; hence both green and blue bands were used to apply ratio transformation algorithms.

Transforms and SDB algorithms

MLR: The MLR analysis between the QGIS SCP processed spectral reflectance values of all three satellite images (all bands as mentioned in Table 1) were regressed against the corresponding depth point of training data points which were well distributed in the study site. The coefficient of determination (R^2) of 0.64, 0.70, and 0.55 was obtained for ASTER/Terra, OLI/Landsat-8 and MSI/Sentinel-2, respectively. The bathymetry product has been generated using coefficients and parameters for validation as shown in Table 2. The SDB derived from MLR has been

Table 2 — The resultant correlation & regression coefficients (method-wise)

Multiple linear regression coefficients for the imageries

ASTER/Terra	*Coeff.*	*Standard error*	*OLI/ LANDSAT-8*	*Coeffi.*	*Standard error*	*MSI/ SENTINEL-2*	*Coeffi*	*Standard error*
Intercept	34.208	2.061	Intercept	-68.151	1.331	Intercept	45.721	0.622
			B2-Blue (OLI)	5.814	0.151	B02-BLUE	277.603	18.268
Band_1- GREEN	-0.211	0.033	B3-Green (OLI)	-5.136	0.157	B03-GREEN	-472.253	14.496
Band_2-RED	-1.610	0.0144	B4-Red (OLI)	-7.840	0.294	B04-RED	426.350	13.008

Calculation of statistical parameters for actual depth vs. SDB

OLI/Landsat-8	R^2: 0.709	RMSE: 5.554 m	MAE: 4.463 m
MSI/Sentinel-2	R^2 : 0.555	RMSE: 5.282 m	MAE: 4.471 m
ASTER/Terra	R^2 :0.645	RMSE: 6.954 m	MAE: 5.816 m

Bathymetry correlated to log ratio transform of Landsat-8 and Sentinel-2

Depth VS Product	*B/G*	*G/R*	*G/B*	*B/R*	*G/NIR*	*R/G*	*R/NIR*	*R/B*	*B/NIR*
Landsat-8	-0.530	0.315	0.433	-0.145	0.315	-0.436	0.101	0.143	-0.043
Sentinel-2	0.52	0.51	-0.51	-0.26	-0.18	0.26	-0.14	0.03	0.14
ASTER	-	0.430	-	-	-0.273	-	-0.523	-	-

Calculation of statistical parameters for actual depth vs. SDB for highlighted transform

OLI/Landsat-8	R^2: 0.41	RMSE: 5.821 m	MAE: 4.876 m
MSI/Sentinel-2	R^2 : 0.2958	RMSE: 6.37 m	MAE: 5.455 m
ASTER/Terra	R^2 :0.6415	RMSE: 5.929 m	MAE: 5.073 m

Bathymetry correlated to SDB products PCA, ICA, and Ratio transform B/G

	OLI/LANDSAT-8			MSI/Sentinel-2			Terra/ASTER
Method	*ICA*	*PCA*	*B/G*	*ICA*	*PCA*	*B/G*	
BLUE	-0.545	-0.278	-0.4703	0.527	0.396		-
GREEN	0.457	0.495		-0.392	0.483	0.307	-
RED	0.222	0.344		-0.181	0.284		-

Calculation of statistical parameters for actual depth vs. SDB for highlighted transform

Data	*Method*	*R^2*	*RMSE*
MSI/Sentinel-2	ICA-BLUE	0.673	3.473 m
OLI/Landsat-8	ICA-BLUE	0.674	3.47 m

plotted against depth points for validation. The relationship between SDB and *in-situ* depth is shown in Figure 3(a).

Log ratio transformation

The Log ratio transformation has been carried out using the Raster Calculator tool in QGIS. The few combinations of bands that have been used are presented in Table 2. The Ratio of blue to the green band for OLI/Landsat-8 &MSI/Sentinel-2 images has shown a higher correlation than other band combinations. However, for ASTER/Terra red to NIR band has shown higher correlations. The best-achieved output transform of each satellite was regressed with *in-situ* bathymetry for the derivation of coefficients. The resulted statistical parameters were used to estimate SDB. The SDB derived has been validated against the test dataset for validation. The relationship between SDB and *in-situ* depth is shown in Figure 3(b).

Log-linear transformation

Lyzenga's univariate Log-Linear transform technique was also applied to each band of all three satellite images. The output transform of each band was correlated to satellite data. The best-correlated transform was regressed against bathymetry to derive SDB. The SDB was validated against the test data set and the resultant R^2, RMSE, and MAE is depicted in Table 2.

Semi-automated tools

The Semi-automated bathymetry product has been derived using Envi 5.3 Software SPEAR, 'The Relative Water Depth tool'. The products of the only first component of PCA transform for each band, ICA transforms for each band, and Ratio algorithm (B/G) have been analysed to correlate with the ground depth, and the result of the correlational analysis is shown in Table 2. The ASTER/Terra imagery was not processed in this tool due to the absence of the blue band, which is mandatory for processing algorithms. The result shows only the blue band ICA of both OLI/Landsat-8 and MSI/Sentinel-2 have a good correlation with bathymetry. Hence, only these two transforms were used to estimate SDB. The estimated SDB was validated against *in-situ* data and the result has been shown in Table 2. Figure 4 shows the graph of the relationship of SDB to the validation dataset.

Machine learning

The efficacy of ML algorithms depends upon large sets of training data. In this univariate ML algorithm, the dataset which consisted of the green band of all three satellites and bathymetry has been split into train data 50 % and test data 50 %. The statistical parameters were retrieved from scikit learn functions. The plot of y-test versus y-predict has been plotted using plugin matplotlib.pyplot. The sns.distplot library was used to plot the density distribution plot of

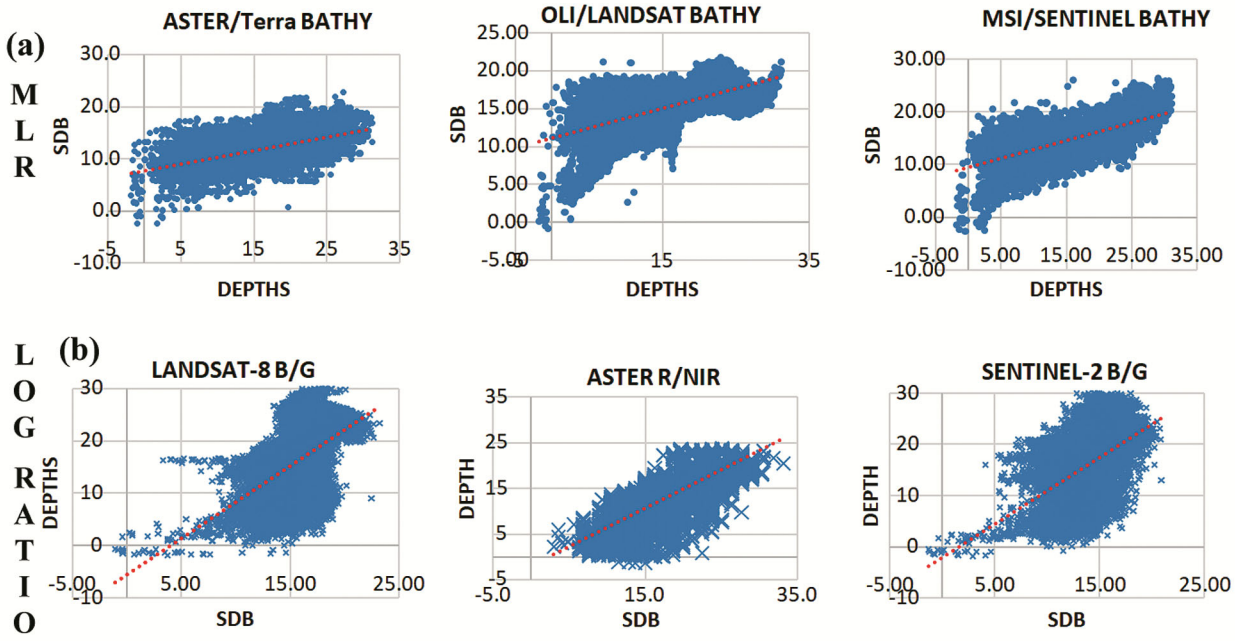

Fig. 3 — Depths versus SDB: (a) MLR method, and (b) Log ratio transformation

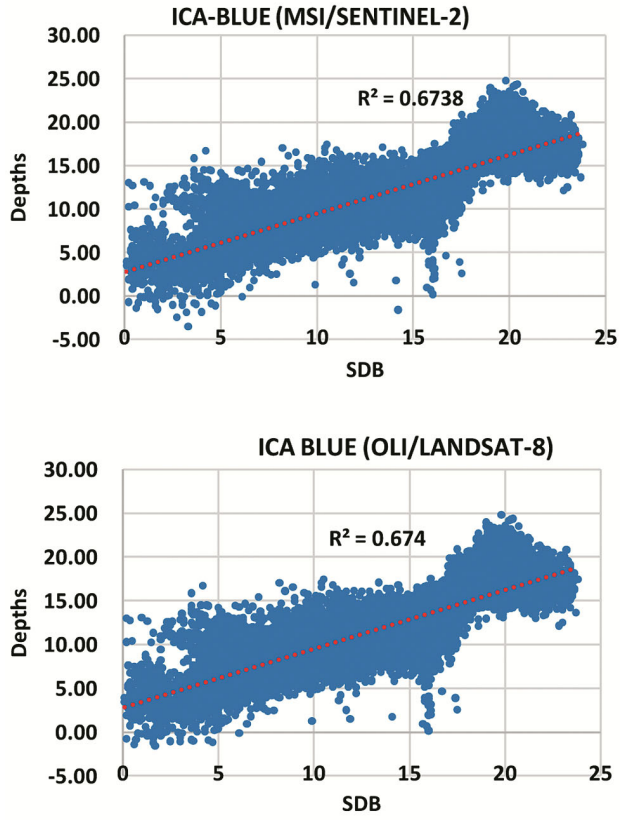

Fig. 4 — Depths versus SDB by ICA (Blue band)

'Actual vs. SDB' as shown in Figure 5. The result of the applied ML algorithm is shown in Table 3.

The overall result of SDB estimation using all the above different transform and algorithms has been summarized in Table 3. It indicates that the OLI/ Landsat-8 provide the best result among the three satellite data sets. Besides, using the ICA transform, the errors can be minimized to the lowest. The lowest RMSE for a depth range of 0 – 32 m is 3.47 m and MAE is 2.854, which is approximately ± 10 % of the depth range.

The best output image of OLI/Landsat-8 is used to carry out the comparative analysis of actual bathymetry to estimate SDB. The SDB map was created using a model derived from the ML algorithm. The Global Mapper software was used to compile maps of the study area as shown in Figure 6. Figure 6(a) shows the Bathymetric map of Vengurla rocks, which has been created using an Inverse Distance weighting (IDW) interpolation raster image using all *in-situ* data points. Figure 6(b) shows the output SDB map derived from the ML algorithm for OLI/Landsat-8 data. Figure 6(c) depicts the difference map by subtracting SDB from actual bathymetry.

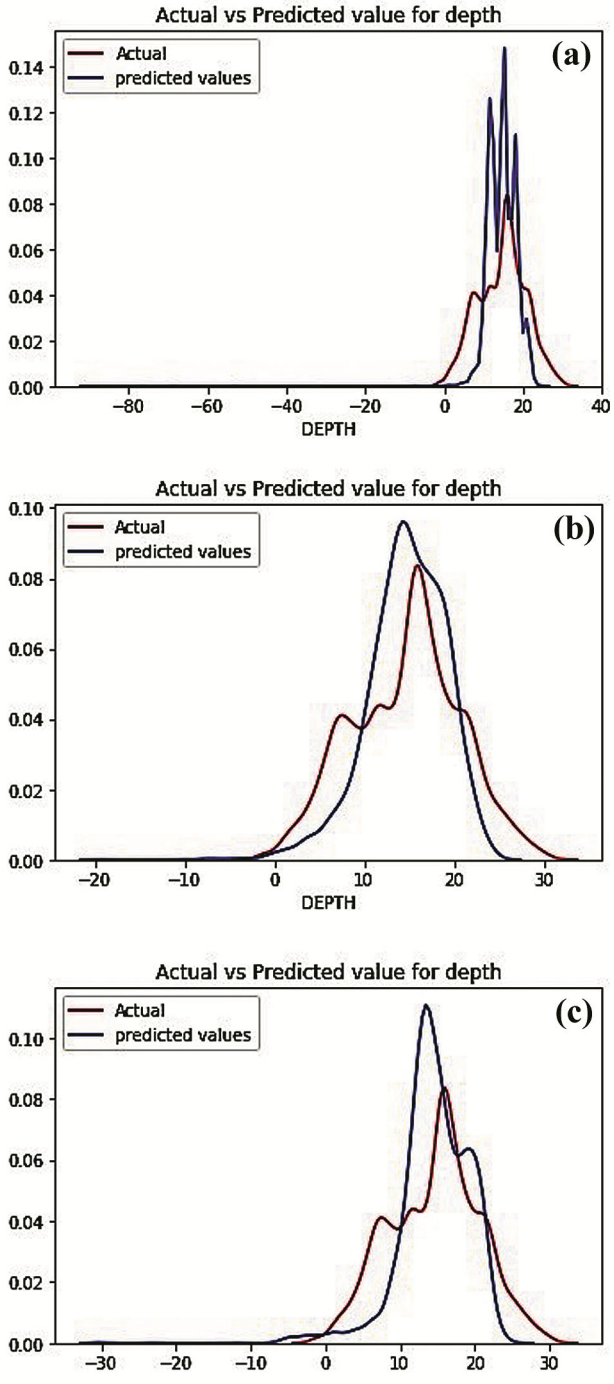

Fig. 5 — Plot of actual depths versus SDB for: (a) ASTER/Terra, (b) MSI/Sentinel, and (c) OLI/Landsat

Discussion

The precise knowledge of bathymetry and seabed terrain is vital for various blue economy opportunities. However, as discussed earlier, carrying out hydrographic surveys in complex regions like Vengurla rocks is difficult and needs huge resources along with

risk to men and material due to the unpredictable nature of coastal terrain. The SDB has been researched for decades as an alternative to bathymetric surveys, but its use remains challenging in turbid water and complex regions. This study attempted estimation of SDB in the study site characterized as highly turbid due to river mouth of Karli River and highly complex due to the presence of several underwater rocks. The initial stage of the research focused on the determination of a suitable band and transform for SDB estimation. The correlation analysis was carried out to select the best suitable band by correlating with the bathymetric dataset with each transform created. The correlations coefficients of the green band were found highly correlated to bathymetry than other bands. This result is consistent with previous remote sensing studies which have explained the attenuation of light in water and the utility of green band 561 nm for SDB[21]. The green band at 561 nm is also highly sensitive to CDOM and detritus in the water and thus, resulted in higher correlations to bathymetry than other bands.

The multivariate regression analysis (Table 2) shows the use of bands in the visible spectrum to derive SDB and R^2 of 0.70 can be achieved by MLR. However, this empirical method produces varying results as the theory of analysis is not grounded in the physics of water optics. The five different transforms were created for applying the SDB algorithm, which includes the two most commonly used Log-linear transform, and Ratio-transform, The PCA and ICA transforms were also created for each band by using semi-automated tools in Envi software. However, only the first components of both these transforms were used which explains most of the variance in the data. All these four transforms of each band were correlated to bathymetry to get the most suitable transform for applying regression to get the SDB algorithm. Table 2 shows the statistical parameters derived and transform used in SDB. The Log-linear transform[3] was more highly correlated to bathymetry than other bands. The Ratio-transform was having low performance indicating ration transform is less

Table 3 — Overall analysis of methods, bands, and their statistical parameters

Sensor/ sdSatellite	Method	Band	R^2	RMSE	MAE
OLI/ Landsat-8	MLR	B,G,R	0.709	5.554 m	4.463 m
	Log ratio	B/G	0.41	5.821 m	4.876 m
	Log linear	B	0.691	4.282 m	3.753 m
	ICA	B	0.674	3.47 m	2.854 m
	ML	G	0.766	3.896 m	-
MSI/ Sentinel-2	MLR	B,G,R,	0.555	5.282 m	4.471 m
	Log ratio	B/G	0.2958	6.37 m	5.455 m
	Log linear	B	0.21	6.97 m	5.11 m
	ICA	B	0.673	3.473 m	2.854 m
	ML	G	0.739	4.0855 m	-
ASTER/ Terra	MLR	G,R	0.645	6.954 m	5.816 m
	Log ratio	R/NIR	0.6415	5.929 m	5.073 m
	Log linear	R	0.556	4.127 m	3.19 m
	ML	G	0.536	5.122 m	-

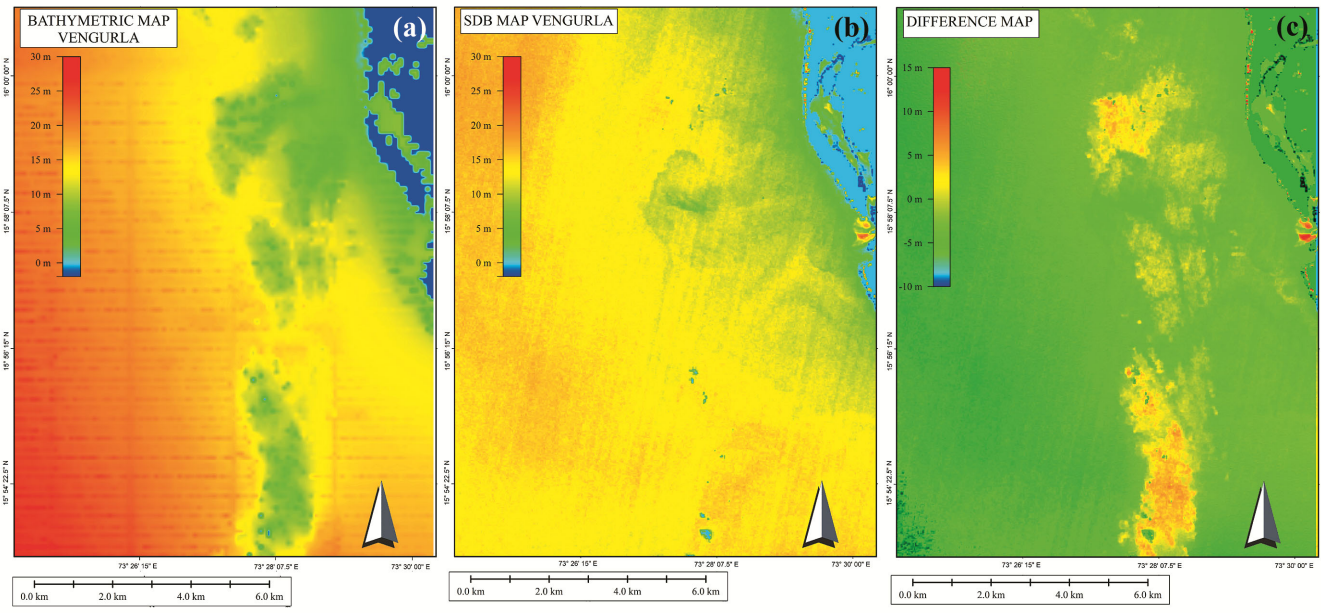

Fig. 6 — (a) Bathymetry map, (b) SDB map, and (c) Difference map (Bathymetry-SDB)

usable in highly turbid water. This is very consistent with the theory of exponential decay of light in water having the varying distribution of dissolved material and turbidity.

The ML algorithm has been applied only on the univariate green band which has resulted in the best predictive accuracy with OLI/Landsat-8 data. This signifies the superiority of ML algorithms in comparison to other methods. Besides, ML algorithms are highly useful when datasets are huge like MBES data which have millions of point samples within a single dataset. The final SDB map was created by applying the ML algorithm to the raster dataset and all 26606 data points were extracted to calculate the histogram and probability plot for actual depth and SDB (Fig. 7). The histogram and probability plot

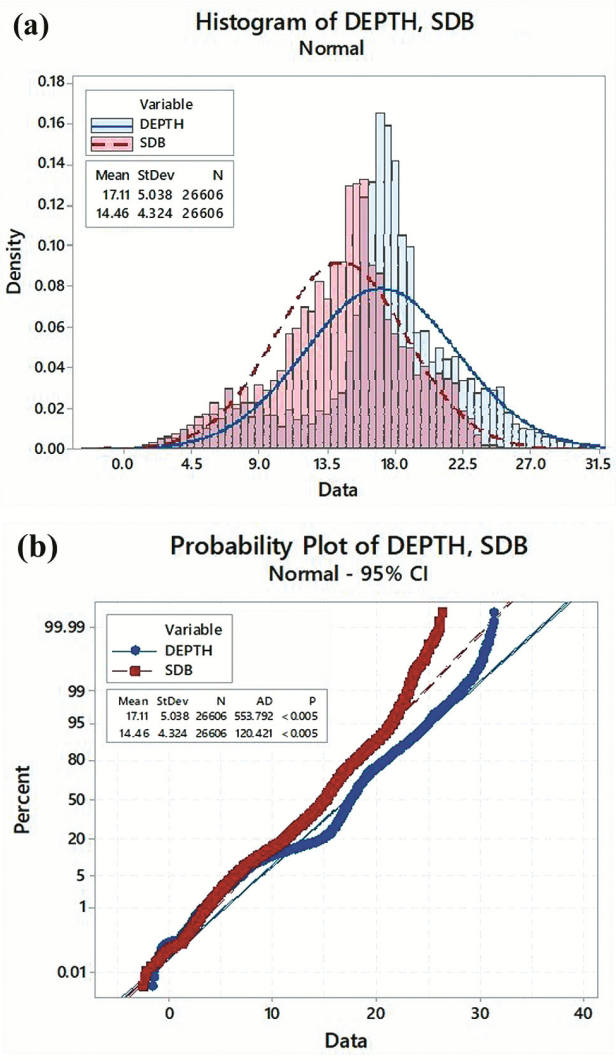

Fig. 7 — (a) Probability plot of SDB vs Bathymetry, and (b) Histogram of SDB vs Bathymetry

reveal prediction up to a depth of 20 m are more accurate, beyond which errors increase significantly.

The Final SDB map was compared with actual bathymetry of the area and a few interesting outcomes were identified. Although, the analysis has displayed RMSE and MAE at 3.4 m and 2.8 m, respectively, most of the geographic region other than the underwater rocks region and river mouth has shown a difference of fewer than 2 m in SDB and bathymetry. The underwater rocky region has depicted a difference of up to 5 m in estimation than actual bathymetry. The very highly turbid region of Karli River mouth was having a difference of more than 10 m in estimation *i.e.*, the algorithm failed drastically in very highly turbid water of the river mouth. This also implies that alone SDB algorithms will not suffice in such highly turbid water, but the water column properties may also be needed for further investigation.

Conclusion

The availability of OLI/Landsat-8 data on the spatial resolution of 30 m, ASTER/Terra data on 15 m, and MSI/Sentinel-2 data on 10 m have made them the choice of most academic researchers in SDB studies. To assess the usability of three data sets, a study has been conducted in a geographically complex, very turbid, navigationally intricate site located with numerous known and unknown navigable dangers. Vengurla rocks site has been examined with two most commonly cited conventional algorithms, log ratio and log-linear transformation, semi-automated (in-built in software packages), and machine learning techniques. The objective of the study was to evaluate the best suitable bands of MS data for SDB estimation in stage one and then apply the most appropriate tools to derive SDB. The open-source tool QGIS SCP has been utilized for pre-processing of data and conversion from radiance to reflectance. DOS atmospheric corrections were applied to the data; however, no significant improvement was observed in the data after applying these corrections.

The SDB product has been derived by using log ratio and linear ratio transformation; PCA, ICA, and ratio transform; and ML regression algorithms. The regression analysis using Jupyter Notebooks executing python script libraries provided better results than other methods. The accuracy of algorithms has been evaluated based on three statistical parameters: RMSE, MAE and R^2. The overall result has indicated that OLI/Landsat-8 provides the best result among the three data sets. Besides, using the independent component

analysis method, the lowest errors can be achieved. The overall analysis of the result suggests that SDB map can be used for reconnaissance of the study site, but can't replace the hydrographic surveys for required International Hydrographic Organization (IHO) accuracy standards of navigational safety.

The limitations of the study include time gaps in the image and *in-situ* data for ASTER/Terra; however, these limitations have not hindered the study's objective. Additional data analysis by segmenting the depth region in different regions is needed. Future research will be focused on statistically determining the SDB parameters by calibrating the satellite data with high-resolution bathymetry and bio-optical parameters in the turbid region.

Conflict of Interest

The authors declare that they have no conflicts of interest.

Ethical Statement

We hereby assure that for the manuscript /insert title/ the following is fulfilled: (a) This material is the authors' own original work, which has not been previously published elsewhere; (b) The paper reflects the authors' own research and analysis in a truthful and complete manner; (c) The paper properly credits the meaningful contributions of co-authors and co-researchers; (d) All sources used are correctly citated; and (e) All authors have been personally and actively involved in substantial work leading to the paper, and will take public responsibility for its content.

Author Contributions

All authors of this paper have contributed in formulating, data processing and writing of this paper. All authors have been personally and actively involved in substantial work leading to the paper, and will take public responsibility for its content.

References

1 Polcyn F C & Rollin R A, Remote sensing techniques for the location and measurement of shallow-water features, *Spacecr Oceanogr Proj*, (1969) 1-80.

2 Polcyn F C & Lyzenga D R, Calculations of water depth from ERTS-MSS data, *ntrs.nasa.gov*, (1973) 1433-1441.

3 Lyzenga D R, Passive remote sensing techniques for mapping water depth and bottom features, *Appl Opt*, 17 (3) (1978) 379-383.

4 Spitzer D & Dirks R W J, Shallow water bathymetry and bottom classification by means of the Landsat and SPOT optical scanners, *SPIE*, 660 (1986) 136-138.

5 Jupp D L B, Mayo K K, Kuchler D A, Claasen D V R, Kenchington R A, *et al.*, Remote sensing for planning and managing the Great Barrier Reef of Australia, *Photogrammetria*, (1985) 4020-4042. doi:10.1016/0031-8663(85)90043-2

6 Stumpf R P, Holderied K & Sinclair M, Determination of water depth with high-resolution satellite imagery over variable bottom types, *Limnol Ocean*, 48 (2003) 547-556.

7 Ashphaq M, Bathymetry estimation in turbid water using SENTINEL-2 image, *Indian Cartogr*, (2017) 381-387.

8 Chaturvedi S K, Srivastava P K & Guven U, A brief review on tsunami early warning detection using BPR approach and post analysis by SAR satellite dataset, *J Ocean Eng Sci*, 2 (2) (2017) 83-89. doi: 10.1016/j.joes.2016.12.001

9 Sakhaee F & Khalili F, Sediment pattern & rate of bathymetric changes due to construction of breakwater extension at Nowshahr port, *J Ocean Eng Sci*, 6 (1) (2021) 70-84. doi: 10.1016/j.joes.2020.04.002

10 Hason M M, Abbood I S & Aldeen O S, Land cover reflectance of Iraqi marshlands based on visible spectral multiband of satellite imagery, *Results Eng*, 8 (2020) 100167. doi: 10.1016/j.rineng.2020.100167

11 Ardakani A H H, Shojaei S, Siasar H & Ekhtesasi M R, Heuristic evaluation of groundwater in arid zones using remote sensing and geographic information system, *Int J Environ Sci Technol*, 17 (7) (2018) pp. 12. doi: 10.1007/s13762-018-2104-1

12 Helber P, Bischke B, Dengel A & Borth D, EuroSAT: A novel dataset and deep learning benchmark for land use and land cover classification, *IEEE J Sel Top Appl Earth Obs Remote Sens*, 12 (7) (2019) 2217-2226.

13 Lyzenga D R, Malinas N P & Tanis F J, Multispectral bathymetry using a simple physically based algorithm, *IEEE Trans Geosci Remote Sens*, 44 (8) (2006) 2251-2259.

14 Noujas V, Kankara R S & Selvan S C, Shoreline management plan for embayed beaches: A case study at Vengurla, west coast of India, *Ocean Coast Manag*, 170 (2019) 51-59. doi: 10.1016/j.ocecoaman.2019.01.001

15 Mahabal A, Pande S, Sharma R M & Pednekar S N, *Status Survey of Indian Edible-Nest Swiftiet Colloealia Unieolor (Jerdon) in Western Ghats, West Coast and Islands in Arabian Sea, India*, Kolkata, 2007.

16 Gao J, Bathymetric mapping by means of remote sensing: methods, accuracy and limitations, *Prog Phys Geogr*, 33 (1) (2009) 103-116. doi: 10.1177/0309133309105657

17 Congedo L, Semi-automatic classification plugin documentation release 6.2.0.1. *Release*, 2019. doi: 10.13140/RG.2.2.29474.02242/1

18 Liceaga-Correa M A & Euan-Avila J I, Assessment of coral reef bathymetric mapping using visible Landsat Thematic Mapper data, *Int J Remote Sens*, 23 (I) (2002) 3-14.

19 Gholamalifard M, Esmaili Sari A, Abkar A & Naimi B, Bathymetric Modeling from Satellite Imagery via Single Band Algorithm (SBA) and Principal Components Analysis (PCA) in Southern Caspian Sea, *Int J Environ Res*, 7 (4) (2013) 877-886.

20 Ceyhun Ö & Yalçın A, Remote sensing of water depths in shallow waters via artificial neural networks, *Estuar Coast Shelf Sci*, 89 (2010) 89-96. doi: 10.1016/j.ecss.2010.05.015

21 Caballero I, Stumpf R P & Meredith A, Preliminary assessment of turbidity and chlorophyll impact on bathymetry derived from Sentinel-2A and Sentinel-3A Satellites in South Florida, *Remote Sens*, 11 (6) (2019) p. 645. doi:10.3390/rs11060645